RSC Advances

PAPER

View Article Online
View Journal | View Issue

Cite this: *RSC Adv.*, 2015, **5**, 54497

Zero-valent iron nanoparticles with sustained high reductive activity for carbon tetrachloride dechlorination†

Ying-Chao Huo,[ab] Wen-Wei Li,*[b] Di Min,[b] Dan-Dan Wang,[a] Hou-Qi Liu,[a] Qin Kong,[a] Tai-Chu Lau[ac] and Raymond J. Zeng*[ab]

Received 19th April 2015
Accepted 15th June 2015

DOI: 10.1039/c5ra07052j

www.rsc.org/advances

Zero-Valent Iron nanoparticles (nZVI) have been extensively applied for the reduction of various recalcitrant organic contaminants, but their reactivity usually declines over time due to the formation of passive iron oxides. In this study we observed a sustained reactivity of nZVI for the dechlorination of carbon tetrachloride (CT) in water during several consecutive reaction cycles. The dechlorination rate constants increased substantially in Cycle 2, then remained at a high level over several consecutive cycles, and ultimately declined in Cycle 7. In the entire process, the solution pH increased only slightly from 7.0 to 7.8, which was different from other unbuffered nZVI reduction systems reported before. Characterization of the particle surface morphology and composition revealed an important role of Fe oxyhydroxide formation in self-buffering the solution pH and sustaining a high nZVI reactivity. Our study provides new knowledge on the nZVI dechlorination process and may offer implications for extending the lifetime of nZVI in wastewater treatment and environmental remediation applications.

1 Introduction

Zero-valent iron nanoparticles (nZVI) have been widely used for environmental remediation and contaminant treatment since the late 1990s,[1] attributed to its high reactivity for reducing a wide range of contaminants in subsurface environments, such as chlorinated organic compounds,[2] nitroaromatic compounds,[3] heavy metals[4] and inorganic compounds.[5] Contamination of groundwater aquifers by halogenated organic compounds (*e.g.*, carbon tetrachloride (CT)) presents a severe threat to today's drinking water security. CT is carcinogenic, highly recalcitrant in the environment and widely exists in the groundwater and soils of many regions.[6] nZVI treatment is an effective and low-cost technology for CT removal. However, a previous study showed that the CT dechlorination kinetics in a pH-buffered solution decreased significantly with the corrosion and surface oxidation of nZVI.[7] While, in other studies, the reductive reactivity of aged nZVI (*i.e.*, a layer of iron oxides naturally formed on nZVI surface) in an unbuffered system increased first with the aging time followed by a gradual decrease, due to a combined effect of original iron oxide shells breakdown and new, non-reactive oxides layer formation.[8] Notably, in that study the dechlorination kinetics seemed to remain at a high level for nZVI with the aging time ranging within 2–5 days, but this phenomenon and the pH dynamics were not given attention by the researchers. Interestingly, another study of nitrate reduction showed that the reaction kinetics of nZVI in an unbuffered solution decreased continuously from 9.34 h^{-1} to 1.64 h^{-1} over a 15 h period without a plateau stage.[9] The solution pH increased rapidly to 9–10 at the reaction beginning and remained almost unchanged throughout the whole reaction process. Based on these findings and the fact that pH could significantly influence dechlorination activity of nZVI,[10] it is thus reasonable to expect that the CT dechlorination kinetics, might be highly related to the solution pH and aging of nZVI. However, no direct evidence has been provided so far. In all, it is still unclear.

In this study, we aim to clarify how solution pH would change during CT reduction by nZVI, and whether nZVI, which would become aged with the reaction proceeding, could remain its activity. The dechlorination kinetics of nZVI during several consecutive reaction cycles were investigated. Impacts of pH and ferrous ion on the reaction kinetics were also evaluated. The variations in surface morphologies and compositions of Fe materials were characterized by scanning electron microscopy (SEM), energy dispersive spectrometer (EDS), X-ray diffraction (XRD) and X-ray photoelectron spectroscopy (XPS). An unusual high reactivity of nZVI and self-buffering solution pH during the

[a]*Advanced Laboratory for Environmental Research & Technology (ALERT), USTC-CityU, Suzhou 215123, China. E-mail: rzeng@ustc.edu.cn; Fax: +8655163601592; Tel: +8655163600203*

[b]*CAS for Unban Pollutant Conversion, Department of Chemistry, University of Science and Technology of China, Hefei 230026, China. E-mail: wwli@ustc.edu.cn; Fax: +8651287161381; Tel: +8651287161361*

[c]*Department of Biology and Chemistry, City University of Hong Kong, Tat Chee Avenue, Kowloon, Hong Kong SAR, Hong Kong, China*

† Electronic supplementary information (ESI) available. See DOI: 10.1039/c5ra07052j

dechlorination process was demonstrated in this study. The underlying mechanisms were elucidated.

2 Materials and methods

2.1 Materials

nZVI was synthesized by reducing 0.3 mol L^{-1} of $FeSO_4 \cdot 7H_2O$ solution with 0.6 mol L^{-1} of $NaBH_4$ solution. The synthesis procedure details and the used chemicals were provided in the ESI.† The synthesized nZVI was washed with deaerated deionized water (DDW) and ethanol followed by filtration. The filtered nZVI particles were vacuum-dried for 12 hours. Ultrapure water (18 MΩ cm, Minipore) was used throughout the experiments.

2.2 CT reductive dechlorination by nZVI

The CT dechlorination experiments were conducted using 250 mL-serum bottles. Prior to the experiment, each bottle was added with 0.05 g nZVI and 100 mL DDW, then immediately bubbled with N_2 (99.9%) for 30 min to ensure anaerobic atmosphere and sealed with Teflon-lined butyl rubber stopper and aluminum crimp cap. To initiate the dechlorination reaction, each bottle was added with 100 μL of CT stock solution (50 mM) prepared in methanol to reach an initial CT concentration of 50 μM. Then, the bottles were put into an orbital shaker at 180 rpm and 30 ± 0.5 °C. After 24 h reaction, each bottle was spiked with another 100 μL of 50 mM CT stock solution to start the next reaction cycle. Seven consecutive dechlorination cycles were performed in this way. The headspace samples of each bottle were collected at given time intervals. To evaluate the possible loss of compounds due to sorption and volatilization, a system without nZVI addition was used as the control. All the experiments were conducted in duplicate.

2.3 Effects of aqueous Fe(II) and pH

The effects of aqueous Fe(II) and pH on the reductive dechlorination of CT were investigated by dosing different concentrations of ferrous chloride ($FeCl_2 \cdot 4H_2O$) and changing the initial pH, respectively. The original solutions contained 50 μL CT and 0.05 g nZVI. The test solutions with different ferrous concentrations (0.14, 0.529 and 5.29 mmol) were denoted as Fe(II)-1, Fe(II)-2 and Fe(II)-3, respectively, and those with initial pH values of 7 and 10 were marked as pH-7 and pH-10.

2.4 Characterization of materials

During nZVI oxidation, changes in morphology and components of Fe oxides/oxyhydroxides on the nZVI surface were identified by SEM, EDS, XRD and XPS. The initial nZVI and the solid samples collected after Cycle 3 (in the high-activity stage) and at the end of the experiment were characterized. More details on instrumentation and sample preparation are provided in the ESI.†

2.5 Analytical methods

Concentrations of CT and its chlorinated products (chloroform (CF) and dichloromethane (DCM)) were determined using headspace analytical technique. Headspace samplings were quantified by an Agilent 6890 gas chromatograph (GC) equipped with an electron capture detector. Methane was measured by a FuLi 9790 GC equipped with a thermal conductivity detector. The concentration of aqueous ferrous was measured using a UV-vis spectrophotometer (Shimadzu UV-1800) at wavelength 510 nm.[11] The solution pH were measured using a pH meter (Mettler Toledo Delta 320). More details on the analytical methods are provided in the ESI.†

2.6 Statistical analyses of kinetics data

One-way ANOVA tests available with SPSS18.0 were performed to analyze the variances of the CT dechlorination kinetics in different reaction cycles in this study. A *p*-value of less than 0.05 indicates a statistically significant difference.

3 Results and discussion

3.1 Pathway of CT reduction by nZVI

The CT concentration decreased while the content of CF, one of its reduction intermediate, gradually increased during the first reaction cycle (Fig. 1). No DCM was detected within the 10 h reaction. In comparison, the nZVI-free control showed no CT degradation. These results indicate that CT was deprived of one chlorine atom by nZVI during the degradation.

Two pathways of CT reductive-transformation have been recognized so far: hydrogenolysis and carbene hydrolysis. Hydrogenolysis can occur through one- or two-electron transfer pathway. One-electron reduction of CT generates a trichloromethyl free radical ($^{\cdot}CCl_3$) that can abstract hydrogen ([H]) to form CF.[12] In the two-electron pathway, the formed $^{\cdot}CCl_3$ is further reduced to obtain a trichloromethyl carbanion

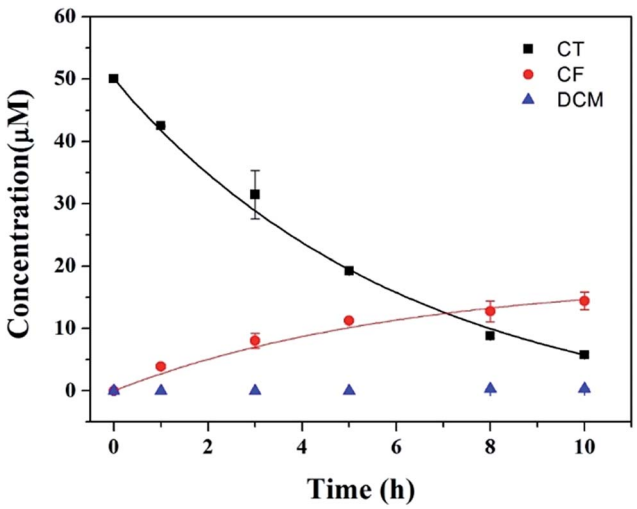

Fig. 1 Reductive degradation of CT by nZVI for the first cycle. Lines show the fits of the data to the model of CT degradation and CF formation. Error bars represent the ranges of duplicate samples.

($[:CCl_3]^-$) and form CF.[13] The formation of trichloromethyl carbanion during the two-electron hydrogenolysis can further undergo α-elimination pathway to form dichlorocarbene ($:CCl_2$) *via* carbene hydrolysis.[14] In this study, generation of DCM was observed only when a complete degradation of CT was achieved. In addition, methane was not detected throughout the experiments (Fig. S1†). Perchloroethylene (PCE) was detected during the degradation (Fig. S1†), which confirms the presence of trichloromethyl free radical.

The kinetics of CT dechlorination and CF formation in the nZVI system can be described by the pseudo-first-order kinetic equation (eqn (1) and (2)).

CT degradation:

$$[\mathrm{CT}]_t = [\mathrm{CT}]_0 \mathrm{e}^{-k_1 t} \quad (1)$$

CF formation:

$$[\mathrm{CF}]_t = A[\mathrm{CT}]_0\left(1 - \mathrm{e}^{-k_1 t}\right); \quad A = \frac{k_2}{k_1} \quad (2)$$

where $[CT]_t$ and $[CF]_t$ are the concentration of CT and CF at sampling time; $[CT]_0$ is the initial CT concentration; k_1 is the observed pseudo-first-order rate constant for CT degradation; k_2 is the rate constant for CF formation, which was calculated using the rate law for parallel first-order formation of reaction products;[15] A is the fraction of CT that is transformed to CF.

The fitting curves of CT degradation and CF formation data are also shown in Fig. 1. The correlation coefficients were both above 0.992, indicating a good fitting between the experimental data and kinetic values. The estimated reduction rate constants in the first reaction cycle were 0.213 h^{-1} for k_1 and 0.058 h^{-1} for k_2.

3.2 Variation of CT degradation kinetics

The CT dechlorination kinetics in several consecutive reaction cycles were investigated and the degradation rate constants were estimated. As shown in Fig. 2, the dechlorination was significantly accelerated in Cycle 2 (0.501 h^{-1}) compared to the first cycle (0.213 h^{-1}). This acceleration should be attributed to a breakdown of the original iron oxide shell of nZVI which resulted in exposure of the active Fe(0) to the contaminants.[16] This depassivation and dissolution of the oxides shell might also explains the distinctly decreased size of the particles after several days of reaction (Fig. 6 and S4†). The rates of hydrogenolysis products (CF and DCM) formation also increased in Cycle 2 correspondingly (Fig. S2†).

Interestingly, the CT degradation rate constants showed no significant variation ($p > 0.05$) during Cycles 2–6, but decreased sharply in Cycle 7. A similar variation trend of CT dechlorination kinetics was observed by Sarathy *et al.*[8] who used nZVI of different aging degrees as the reductive agent. In our study, the aging process occurred spontaneously over the reaction process and pH was not controlled, which can better reflect the real process of nZVI corrosion in natural environment.

The reductive chlorination activity of ZVI is governed by the iron surface components and properties. Notably, anaerobic dechlorination (eqn (3)) and hydrolysis (eqn (4)) are usually accompanied with pH increase and ferrous ions accumulation, which might in turn affect the dechlorination kinetics.

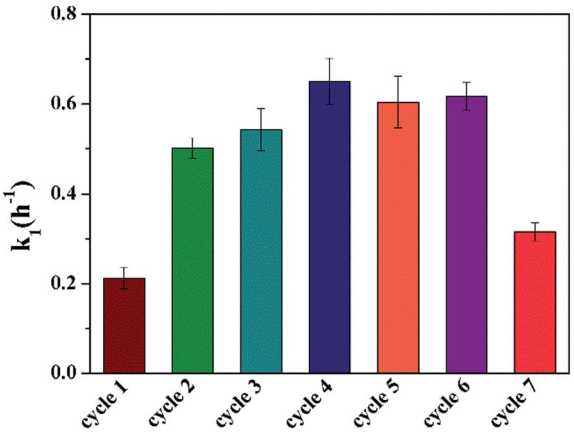

Fig. 2 Reductive dechlorination kinetics of CT by nZVI for seven cycles. Error bars are the ranges of duplicate samples.

$$\mathrm{Fe}^0 + \mathrm{R{-}Cl} + \mathrm{H}^+ \rightarrow \mathrm{Fe}^{2+} + \mathrm{R{-}H} + \mathrm{Cl}^- \quad (3)$$

$$\mathrm{Fe}^0 + 2\mathrm{H}^+ \rightarrow \mathrm{Fe}^{2+} + \mathrm{H}_2 \quad (4)$$

3.3 Variations of pH and ferrous ions

To understand the unusual changes of dechlorination kinetics, the variations of pH and ferrous ions in solution during CT dechlorination were monitored, Fig. 3a shows that the solution pH changed only slightly, suggesting that the system was capable of self-buffering. Meanwhile, the ferrous ions concentration was increased continuously.

It is known that the solution pH could substantially affect the reaction products[18] and species of formed Fe oxides.[19] On the other hand, the ferrous accumulated during the reaction might play multiple roles in affecting the system reductive activity. For instance, Fe(II) adsorbed on iron oxides could directly reduce a variety of pollutions.[20] However, deposition of some iron oxides on the nZVI surface could also significantly block the electron transfer and decrease the reaction activity. To clarify the intercorrelations between pH and ferrous ion and their roles in dechlorination, the CT degradation under different ferrous concentration and initial pH conditions were tested.

Fig. 4a shows that CT was completely dechlorinated within 3 h for Fe(II)-3, while it took 8 and 10 hours for Fe(II)-2 and Fe(II)-1 respectively, and no CT dechlorination occurred in the nZVI-free system. This result suggests that, although ferrous ions itself cannot reduce CT, the CT degradation rate was positively correlated to the ferrous concentration when nZVI was present. The final pH of the mixtures were 8.7, 8.2 and 7.7 for Fe(II)-1, Fe(II)-2, Fe(II)-3, respectively (Fig. 4b). The inverse correlation between pH and the added ferrous amount might be due to: (1) ferrous combines with hydroxide ion to form iron oxides and oxyhydroxides, resulting in decreased OH^- concentration; (2) ferrous leads to proton release by substituting the H atom of Fe oxyhydroxides (reactions (5) and (6)).[21]

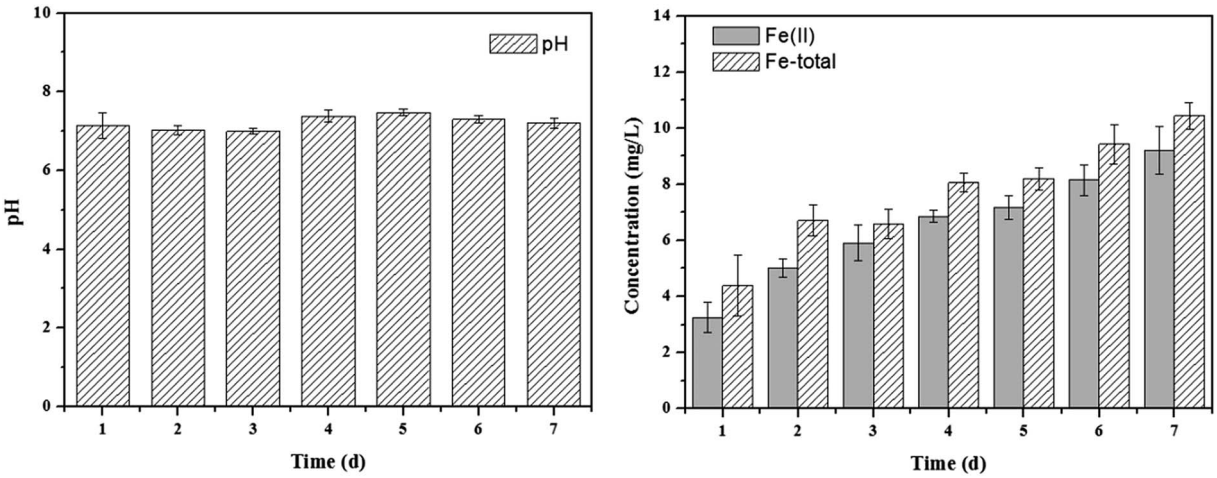

Fig. 3 The variation of pH and ferrous during the CT dechlorination by nZVI.

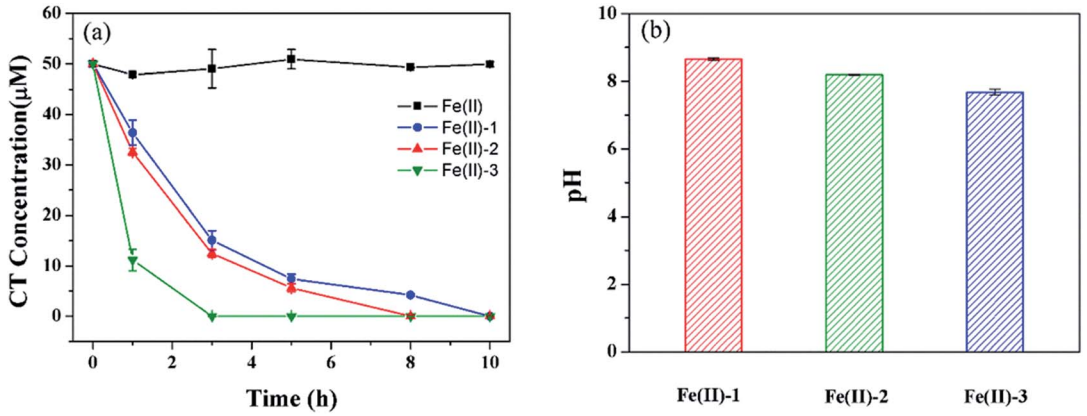

Fig. 4 (a) CT reductive dechlorination by nZVI with different addition of ferrous and (b) the final pH. Error bars are the ranges of duplicate samples.

$$\equiv FeOH + Fe^{2+} \leftrightarrow FeOFe(II)^{+} + H^{+} \quad (5)$$

$$\equiv FeOH_2^{+} + Fe^{2+} \leftrightarrow FeOFe(II)^{+} + 2H^{+} \quad (6)$$

According to the above mechanism, the continously-generated ferrous during the dechlorination might serve as an effective buffer to neutralize the alkali produced from nZVI corrosion, thereby sustaining a stable pH in the entire reaction process (Fig. 3). This self-buffered pH due to formation of iron oxyhydroxides might also be one important reason for the sustained high dechlorination activity of nZVI over the consecutive reaction cycles. As evidenced in Fig. 5, significantly higher CT dechlorination rate was obtained in neutral pH system (0.211 h^{-1} for pH-7 *versus* 0.110 h^{-1} for pH-10). Under alkaline condition, the dechlorination thermodynamics becomes less favorable and meanwhile a thick iron oxides coat would be built on the particle surface, severely blocking the electron transfer from the iron core.[9,22,23]

3.4 Characterization of nZVI and formed ion oxides

Characterization of the solid-phase samples collected at different reaction stages confirms the formation of iron oxyhydroxides during the consecutive dechlorination cycles.

SEM examination revealed that the initial nZVI contained abundant nanosphere clusters (Fig. 6a), which was typical of nZVI particles. The nanosphere sizes were in the range of 50–200 nm. The EDS result clearly showed the elemental mapping of Fe and O in the nanonecklace structure (Fig. 6b), implying that the nZVI used in our study was slightly oxidized. This happens frequently during the synthesis, drying, storage and application processes, where nZVI with high activity could be easily oxidized to form a thin layer of iron oxides on the surface when exposed to the atmosphere or water. However, the morphology and components of nZVI changed significantly after three dechlorination cycles. Both the number and size of nanospheres decreased, while large amount of platy Fe oxide minerals with bulk and laminated structures were formed (Fig. 6c and S4b†). Notably, the particle area and the bulk

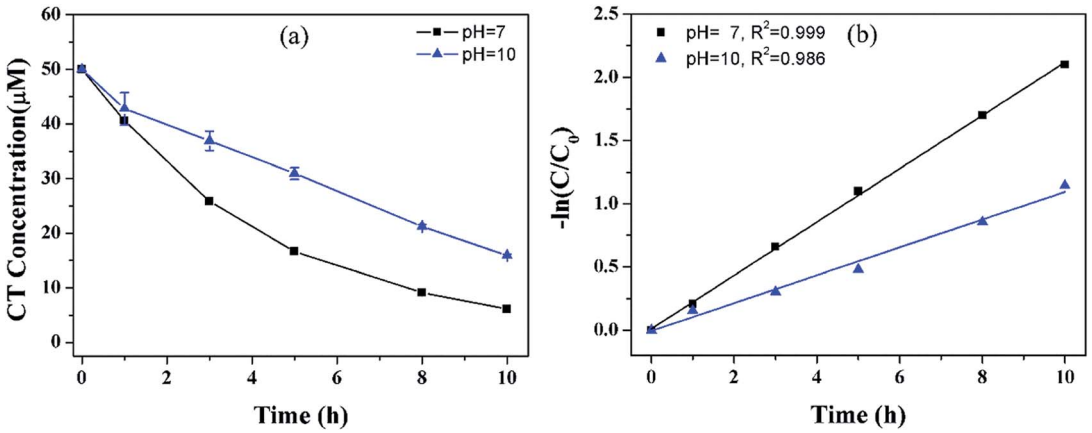

Fig. 5 (a) Profiles of CT concentration as a function of reaction time during the anaerobic dechlorination by nZVI with different initial pH. Error bars are the ranges of duplicate samples. (b) Degradation kinetics of CT with different initial pH (7 and 10).

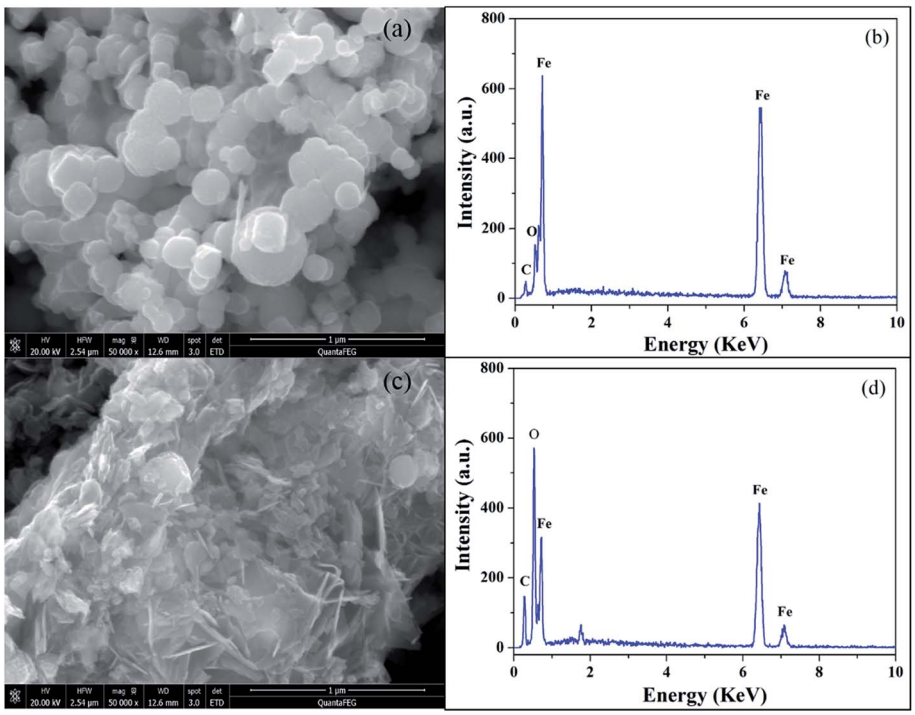

Fig. 6 (a) SEM image and (b) EDS analysis of initial nZVI; (c) SEM image and (d) EDS analysis of aged nZVI after Cycle 3.

mineral area showed no significant difference in the iron and oxygen contents, indicating a similar composition of the iron hydroxides on the particle surface in the precipitate (Fig. S4b†). In addition, the EDS data showed that the oxygen content increased from 6% in the initial nZVI to 25% after Cycle 3 (Fig. 6b and d). These results confirm that Fe oxyhydroxides were formed accompanied with the continuous ZVI corrosion. These newly-formed porous Fe oxides posed insignificant impacts on the corrosion of the ZVI particles and might even directly contribute to CT dechlorination by utilizing the adsorbed Fe(II).[17] At the end of the experiment, more bulk and dense-structured iron precipitates were observed, which might hamper the electron transfer from the buried particles ZVI particles (Fig. S3 and S4†).

The variations of nZVI composition during reaction were validated by XRD and XPS. Pure Fe, with the XRD peaks of 44.9 and 65.0°, was identified for the initial nZVI Fe (Fig. 7a). However, the XRD signal was weak, indicating a relatively low crystallinity. Meanwhile, no distinct peaks of iron oxides were observed, implying a small amount or poor crystallinity of the oxides shell.[24] The XPS spectra revealed that only elements Fe, O, and C existed in the original nZVI (Fig. S5a†). The C1s peak at 284.8 eV should be attributed to the adventitious carbon (Fig. S5b†). For the original nZVI, two narrow distinct peaks of

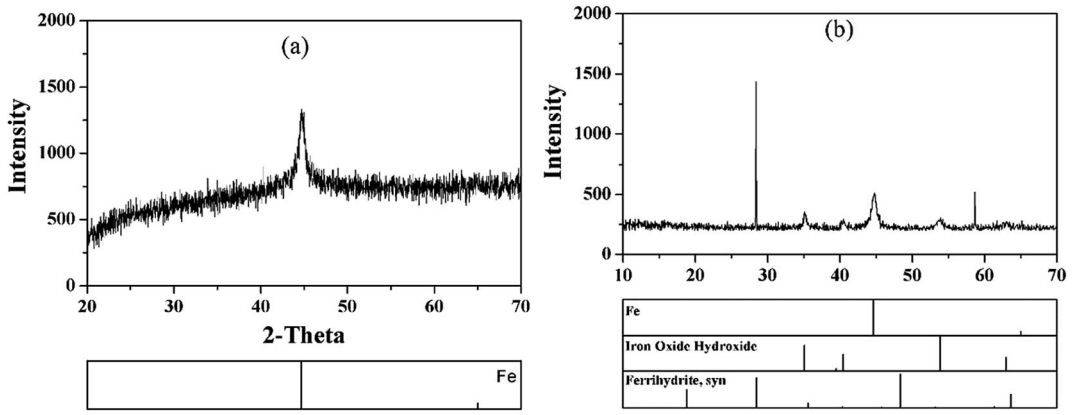

Fig. 7 XRD analysis of (a) initial nZVI and (b) after Cycle 3.

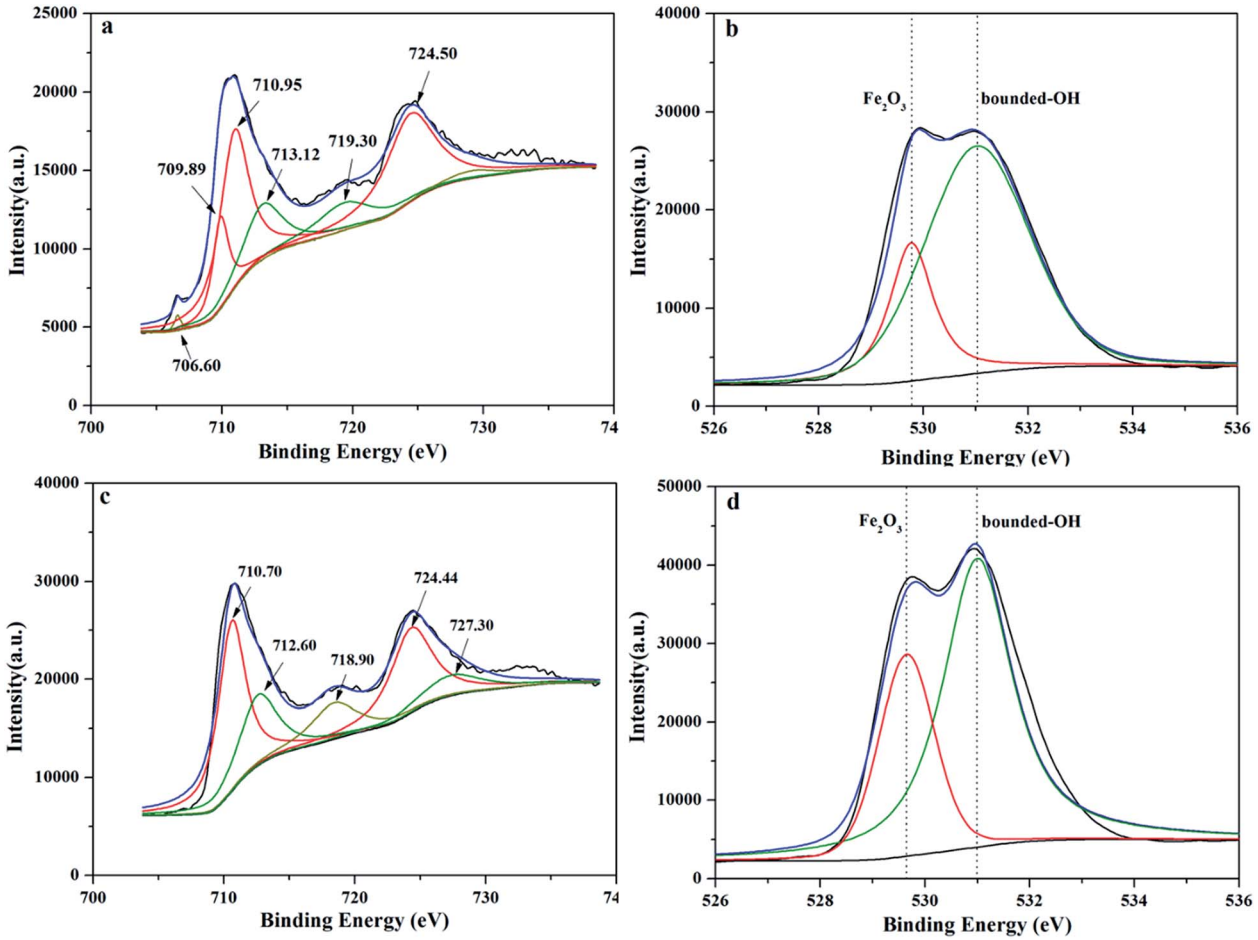

Fig. 8 High resolution XPS spectra of (a) Fe2p and (b) O1s for initial nZVI; high resolution XPS spectra of (c) Fe2p and (d) O1s for aged nZVI after Cycle 3.

similar intensity, 709.89 eV and 710.95 eV, separated by about 1 eV were detected (Fig. 8a). The peak positions were consistent with the literature values of 709.7 and 710.8 eV assigned to Fe2p3/2 for α-Fe_2O_3. Two other prominent peaks also occurred, which are ascribed to a satellite band at 719.30 about 8 eV above the Fe (2p3/2) line and the shoulder peak at 724.50 eV in the high resolution spectra.[25] These data confirm that the oxide shells of the Fe(0) core were Fe_2O_3. Besides the predominant peaks of Fe in Fe_2O_3, a peak at a low binding energy of 706.9 eV, attributed to Fe2p1/2 in pure Fe, was also detected, indicating that the thickness of the Fe_2O_3 shell was less than 10 nm since

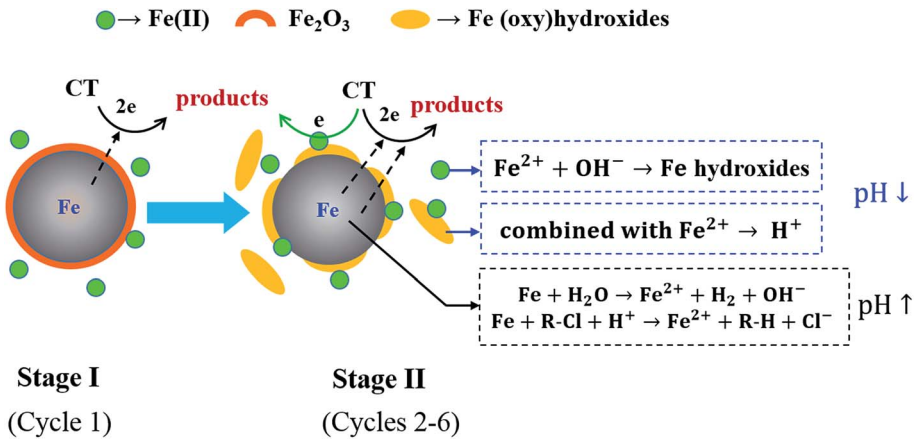

Fig. 9 Hypothesized mechanism of sustained CT dechlorination activity of nZVI over consecutive reaction cycles.

the XPS could only detect the photoelectrons from the outer surface of 10 nm.

After three CT dechlorination cycles, obvious peaks of iron oxides and oxyhydroxides occurred while the peaks of Fe(0) remained, suggesting a significant change of the iron oxides composition. It has been reported that certain iron oxides/oxyhydroxides, such as green rust, ferrihydrite and magnetite, could promote the reductive transformation of contaminants.[26,27] The evolution of surface chemical compositions of nZVI during the reaction was further convinced by XPS analysis. The peaks of pure iron disappeared after Cycle 3 (Fig. 8c), likely due to decreased Fe(0) content and the inclusion of Fe particles within the Fe oxides matrixes. The high-resolution XPS spectra of O1s could be fitted by two peaks at binding energies of about 529.77 and 531.02 eV, respectively (Fig. 8b and d). The dominant peak at 529.77 eV is assigned to the lattice oxygen of Fe (Fe_2O_3), while the other O1s peaks at around 531.02 eV is ascribed to adsorbed hydroxyl (Fe-OH_{ad}), lattice hydroxyl (Fe-$OH_{lattice}$) and water (H_2O),[28] which we denoted as bonded-OH here. It is obvious that the bounded-OH content increased during the dechlorination, which is in accordance with the strengthened signals of Fe oxyhydroxides detected by XRD (Fig. 7b).

With the further proceeding of dechlorination reactions, other ion oxides such as magnetite, hematite and goethite also occurred at the end of the experiments, as demonstrated by the XRD data (Fig. S6†). The formation of these iron oxides could suppress the reduction of chlorinated organics.[29] Therefore, these inactive iron oxides might form a matrix of dense structure and block the electron transfer from the buried nZVI particles. In addition, the amount of nZVI might become limiting at this stage due to continuous consumption. Thus, the decreased nZVI amount might also account for the decreased dechlorination kinetics at Cycle 7.

3.5 Mechanisms of sustained high dechlorination activity of nZVI

Based on the above analysis, we propose the following mechanisms of the sustained high dechlorination activity of nZVI (Fig. 9). In the intial reaction (Cycle 1), CT reduction was mainly driven by the Fe(0) core of nZVI. However, the electrons from Fe(0) core have to pass through an iron oxide shell. This oxide shell increased the electron transfer resistance and resulted in relatively low dechlorination kinetics. With the proceeding of reaction, this oxide shell is broken down and meanwhile some loose-structured, permeable active oxides precipitates are formed and deposited both on the particle surface and in the bulk solution (Fig. S4†). As a consequence, more Fe(0) are exposed and become available for direct CT reduction. In the meantime, the newly-formed Fe oxyhydroxides don't significantly block the electron flow from inner Fe(0), and may even directly participate in the dechlorination by utilizing the active adsorbed Fe(II).[30,31] Another important factor is that the formation of Fe oxyhydroxides resulted in a self-buffering of solution pH. On one hand, the corrosion of nZVI and reductive dechlorination results in more ferrous generation and increased pH (eqn (3) and (4)). On the other, the generated ferrous continuously consumes alkali by directly combining with OH^- to form oxyhydroxides and further complexing with the oxyhydroxides to release H^+. All the above factors together result in a stable pH and sustained dechlorination kinetics over several reaction cycles. Notably, the amount and size of Fe(0) particles would decrease over time due to the continuous consumption (Fig. S4†). In the meantime, the amount, composition and structure of the Fe oxyhydroxides would gradually change, resulting in less active oxyhydroxides and higher electron transfer resistance. These factors might eventually lead to decreased dechlorination kinetics by nZVI during long-time reaction.

4 Conclusions

The present study demonstrates that nZVI can be efficiently used for reductive dechlorination of CT with a pH self-buffering ability and sustained high activity. A breakdown of the original oxide shell and meanwhile the generation of a more active, porous oxyhydroxides contributed to the significantly accelerated dechlorination compared to the initial nZVI. The formation of Fe oxyhydroxides was also an important reason of the pH

self-buffering in our system. However, the dechlorination kinetics eventually declined after long-time reaction due to decreased Fe(0) amount and changes of the Fe oxyhydroxides composition and structure. These findings imply a high potential to maintain a high activity of nZVI in natural environment by controlling appropriate pH and ferrous level, and may provide implications for *in situ* remediation of chlorinated contaminants and other oxidative species in subsurface environment.

Acknowledgements

The authors wish to thank the National Nature Science Foundation of China (51278479), the National 863 Project (2011AA060901), the Hundred-Talent Program of Chinese Academy of Sciences, the Program for Changjiang Scholars and Innovative Research Team in University, the Fundamental Research Funds for the Central Universities (wk2060190040), the Collaborative Innovation Center of Suzhou Nano Science and Technology, and the Hong Kong University Grants Committee (AoE/P-03-08) for the financial support of this work.

References

1 D. O'Carroll, B. Sleep, M. Krol, H. Boparai and C. Kocur, *Adv. Water Resour.*, 2013, **51**, 104–122.
2 M. Zhang, F. He, D. Zhao and X. Hao, *Water Res.*, 2011, **45**, 2401–2414.
3 Y. Mu, H. Q. Yu, J. C. Zheng, S. J. Zhang and G. P. Sheng, *Chemosphere*, 2004, **54**, 789–794.
4 L. N. Shi, X. Zhang and Z. L. Chen, *Water Res.*, 2011, **45**, 886–892.
5 S. R. Kanel, B. Manning, L. Charlet and H. Choi, *Environ. Sci. Technol.*, 2005, **39**, 1291–1298.
6 C. Penny, S. Vuilleumier and F. Bringel, *FEMS Microbiol. Ecol.*, 2010, **74**, 257–275.
7 S. Bae and W. Lee, *Environ. Sci. Technol.*, 2014, **48**, 2368–2376.
8 V. Sarathy, P. G. Tratnyek, J. T. Nurmi, D. R. Baer, J. E. Amonette, C. L. Chun, R. L. Penn and E. J. Reardon, *J. Phys. Chem. C*, 2008, **112**, 2286–2293.
9 K. Sohn, S. W. Kang, S. Ahn, M. Woo and S.-K. Yang, *Environ. Sci. Technol.*, 2006, **40**, 5514–5519.
10 Y. Liu and G. V. Lowry, *Environ. Sci. Technol.*, 2006, **40**, 6085–6090.
11 Z. Ai, Z. Gao, L. Zhang, W. He and J. J. Yin, *Environ. Sci. Technol.*, 2013, **47**, 5344–5352.
12 H. J. Ahr, L. J. King, W. Nastainczyk and V. Ullrich, *Biochem. Pharmacol.*, 1980, **29**, 2855–2861.
13 J. Hine, R. C. Peek Jr and B. D. Oakes, *J. Am. Chem. Soc.*, 1954, **76**, 827–829.
14 M. L. McCormick and P. Adriaens, *Environ. Sci. Technol.*, 2004, **38**, 1045–1053.
15 Y. T. Lin and C. Liang, *Environ. Sci. Technol.*, 2013, **47**, 3299–3307.
16 J. T. Nurmi, P. G. Tratnyek, V. Sarathy, D. R. Baer, J. E. Amonette, K. Pecher, C. Wang, J. C. Linehan, D. W. Matson and R. L. Penn, *Environ. Sci. Technol.*, 2005, **39**, 1221–1230.
17 J. Filip, F. Karlický, Z. Marušák, P. Lazar, M. Černík, M. Otyepka and R. Zbořil, *J. Phys. Chem. C*, 2014, **118**, 13817–13825.
18 K. M. Danielsen and K. F. Hayes, *Environ. Sci. Technol.*, 2004, **38**, 4745–4752.
19 H. Y. Jeong, K. Anantharaman, S. P. Hyun, M. Son and K. F. Hayes, *Water Res.*, 2013, **47**, 6639–6649.
20 J. E. Amonette, D. J. Workman, D. W. Kennedy, J. S. Fruchter and Y. A. Gorby, *Environ. Sci. Technol.*, 2000, **34**, 4606–4613.
21 T. Liu, X. Li and T. D. Waite, *Environ. Sci. Technol.*, 2013, **47**, 13712–13720.
22 N. Sato, T. Noda and K. Kudo, *Electrochim. Acta*, 1974, **19**, 471–475.
23 T. L. Johnson, W. Fish, Y. A. Gorby and P. G. Tratnyek, *J. Contam. Hydrol.*, 1998, **29**, 379–398.
24 L. Lu, Z. Ai, J. Li, Z. Zheng, Q. Li and L. Zhang, *Cryst. Growth Des.*, 2007, **7**, 459–464.
25 N. McIntyre and D. Zetaruk, *Anal. Chem.*, 1977, **49**, 1521–1529.
26 M. Erbs, H. C. B. Hansen and C. E. Olsen, *Environ. Sci. Technol.*, 1999, **33**, 307–311.
27 R. A. Doong, C. C. Lee and C. M. Lien, *Chemosphere*, 2014, **97**, 54–63.
28 X. Zhou, J. Lan, G. Liu, K. Deng, Y. Yang, G. Nie, J. Yu and L. Zhi, *Angew. Chem., Int. Ed. Engl.*, 2012, **51**, 178–182.
29 J. Farrell, M. Kason, N. Melitas and T. Li, *Environ. Sci. Technol.*, 2000, **34**, 514–521.
30 J.-L. Chen, S. R. Al-Abed, J. A. Ryan and Z. Li, *J. Hazard. Mater.*, 2001, **83**, 243–254.
31 M. Elsner, R. P. Schwarzenbach and S. B. Haderlein, *Environ. Sci. Technol.*, 2004, **38**, 799–807.

